Finding a suitable chest x-ray image size for the process of machine learning to build a model for predicting Pneumonia

Kriengsak Yothapakdee [a,1,*], Yosawaj Pugtao [b,2], Sarawoot Charoenkhum [c,3], Tanunchai Boonnuk [d,4], Kreangsak Tamee [e,5]

[a] Department of Computer Science, Faculty of Science and Technology, Loei Rajabhat University, Loei, Thailand
[b] Internal Medicine Department, Chumphae Hospital, Chum Phae District, Khon Kaen, Thailand
[c] Hospital Director of Khok-Nong-Kae, Health Promoting Hospital of Wangsaphung District, Loei, Thailand
[d] Department of Public Health, Faculty of Science and Technology, Loei Rajabhat University, Loei, Thailand
[e] Department of Computer Science and Information Technology, Faculty of Science, Naresuan University, Phitsanulok, Thailand
[1] kriengsak@lru.ac.th; [2] tarmd7@gmail.com; [3] sarawoot39283@gmail.com; [4] tanunchai.boo@lru.ac.th; [5] kreangsakt@nu.ac.th
* corresponding author

ARTICLE INFO

Article history
Received December 16, 2024
Revised February 9, 2025
Accepted February 10, 2025
Available online February 28, 2025

Keywords
Chest X-ray
Suitable size
Covid-19
Machine learning
Predictive model

ABSTRACT

This study focused on algorithm performance and training/testing time, evaluating the most suitable chest X-ray image size for machine learning models to predict pneumonia infection. The neural network algorithm achieved an accuracy rate of 87.00% across different image sizes. While larger images generally yield better results, there is a decline in performance beyond a certain size. Lowering the image resolution to 32x32 pixels significantly reduces performance to 83.00% likely due to the loss of diagnostic features. Furthermore, this study emphasizes the relationship between image size and processing time, empirically revealing that both increasing and decreasing image size beyond the optimal point results in increased training and testing time. The performance was noted with 299x299 pixel images completing the process in seconds. Our results indicate a balance between efficiency, as larger images slightly improved accuracy but slowed down speed, while smaller images negatively impacted precision and effectiveness. These findings assist in optimizing chest X-ray image sizes for pneumonia prediction models by weighing diagnostic accuracy against computational resources.

1. Introduction

Pneumonia is a severe infectious disease that affects the lower respiratory system, caused by inflammation of the alveoli in the lungs. The disease can be triggered by various pathogens, including fungi, bacteria, and viruses [1], [2]. According to the World Health Organization (WHO), pneumonia remains a significant global health issue, particularly in developing countries, and it contributes to a considerable number of deaths, especially among children under the age of five [3]. In addition to the unfortunate events mentioned above to emphasize the significant nature of pneumonia as a global health threat. The emergence of coronavirus disease 2019 (COVID-19) has also led to an increase in respiratory infections worldwide. The COVID-19 pandemic, caused by the SARS-CoV-2 virus, has led to an unprecedented global public health crisis [4]. The virus primarily attacks the respiratory tract, resulting in acute lung injury where the alveoli fill with pus and fluid when a person has pneumonia, causing difficulty breathing and limiting oxygen consumption, and in severe cases, acute respiratory distress syndrome (ARDS), resulting in significantly increased morbidity and mortality [5].

As the novel coronavirus disease (COVID-19) continues its global spread, researchers employ a range of methodologies to decipher the virus's biology and identify factors influencing its evolution and outbreak patterns. Phylogenetic and phylodynamic approaches are pivotal in this endeavor, enabling scientists to trace the virus's transmission pathways and understand its evolutionary dynamics. These methods involve analyzing genetic sequences from diverse SARS-CoV-2 samples worldwide, facilitating the reconstruction of the virus's spread, and identifying mutations that may affect transmissibility or virulence. The study has provided an important foundation for developing measures that the WHO has implemented to control the spread of COVID-19. They have used data from analyzing virus strains and tracking the spread of the virus in different regions. The WHO has recommended guidelines and control measures, including social distancing, wearing face masks, self-isolation, travel restrictions, and patient screening. These measures have been specifically designed to control the spread of the virus and minimize the risk of infection on a global scale [6]. Over the past five years, the WHO declared COVID-19 no longer a public health emergency of international concern (PHEIC) on May 5, 2020 [7], highlighting a decreased number of infections, hospitalizations, deaths, ICU admissions, and ubiquitous immunization against the virus [8]. However, this announcement does not mean that the world is free from coronavirus-2019 because new strains of the virus are constantly emerging and being discovered nowadays [9]. And they remain a major threat to the world's social and economic systems. A variety of screening techniques and diagnostic procedures provide surveillance strategies. It is essential for finding and isolating affected individuals, which helps to stop the spread of the virus. In addition, screening initiatives enable early identification of new strains, allowing rapid adjustments to immunization programs and public health regulations to effectively deal with problems caused by the virus.

A chest X-ray (CXR) is a widely utilized diagnostic imaging technique that employs X-rays to produce detailed images of the organs within the thoracic cavity, including the lungs, heart, and ribs. This non-invasive procedure provides clinicians with an efficient means of detecting and evaluating abnormalities in these structures. It is particularly valuable in diagnosing pneumonia, a condition characterized by inflammation of the lung tissue, typically resulting from an infectious etiology. Chest X-rays are essential for identifying key indicators of pneumonia, such as pulmonary inflammation, fluid accumulation, and infection, which can aid in assessing the extent and severity of the condition. This information is crucial for guiding treatment decisions and determining the appropriate management course. Additionally, CXR monitors treatment progression and evaluates the patient's recovery. Recent clinical guidelines have recommended CXR as the initial imaging modality for patients with suspected pneumonia, underscoring its role in effective clinical decision-making [10].

Machine learning (ML) has revolutionized the analysis of medical images, particularly chest X-rays (CXRs), by enhancing diagnostic accuracy and efficiency. ML algorithms, especially deep learning models, play a critical role in automating CXR interpretation, enabling the detection of various thoracic conditions, including pneumonia, tuberculosis, and lung cancer. These models identify subtle patterns in large datasets, improving diagnostic precision. ML also reduces the workload for radiologists, allowing them to focus on complex cases, while promoting early detection of abnormalities and timely interventions that can improve patient outcomes. Recent advancements in ML, such as self-supervised learning models like EVA-X [11], have furthered the generalization of CXR analysis across multiple diseases. Additionally, the fusion of convolutional neural networks (CNNs) [12] and vision transformers has resulted in more accurate multi-label chest X-ray classification. These developments demonstrate the scalability of ML systems, enabling access to high-quality diagnostic support in settings with limited radiological expertise. As ML continues to evolve, it holds the potential to significantly enhance diagnostic capabilities, early detection, and patient care, especially in resource-constrained environments.

However, previous studies have suggested that determining an appropriate image resolution is critical for improving machine learning performance in medical imaging, with higher resolution chest X-ray (CXR) images improving classification accuracy [13], whereas studies on tuberculosis lesion segmentation have shown that increasing image resolution does not always yield better results [14]. In our study, we look at the impact of CXR image size on the trade-off between image detail and computational efficiency to improve diagnostic accuracy. The findings are intended to help develop more efficient and resource-efficient AI-powered medical imaging applications.

2. Method

We divide the research methodology into the following parts: examining the sample size and number of medical images in each study, and a popular machine learning algorithm for classifying different types of medical images.

2.1. The Size and Amount of Medical Images

According to the previous literature review, medical imaging has been widely used in research and development, with differences in the size and number of samples depending on the purpose and goals of each research project, as shown in Table 1.

Table 1. Review summary of chest X-ray image size for developing a model

Researcher	Details		
	Size of images (pixel)	*Number of images (instances)*	*Medical image type*
Olar *et al.* [15]	512x512	1589	X-ray
Pal *et al.* [16]	224x224	6432	X-ray
Baik *et al.* [17]	512x512	23712	X-ray
Ukwuoma *et al.* [18]	299x299	14400	X-ray
Reddy *et al.* [19]	512x512, 1024x1024	1818	X-ray
Liu and Shen [20]	28x28, 56x56, 112x112, 224x224	30386	X-ray
Chen *et al.* [21]	224x224, 299x299	21165	X-ray
Echtioui and Ayed [22]	224x224	15156	X-ray
Abdullah *et al.* [23]	150x150	9220	X-ray
Akyol [24]	224x224	16360	X-ray
Moris *et al.* [25]	4892x4020, 948x1130, 2048x2048	1047	X-ray
Asif *et al.* [26]	256x256	3886	X-ray
Shastri *et al.* [27]	224x224	1045	X-ray
Hayat *et al.* [28]	128x128, 224x224, 229x229	17599	X-ray
Alghamdi *et al.* [29]	256x256, 512x512, 1024x1024	3555	X-ray
Kanjanasurat *et al.* [30]	512x512	16210	X-ray
Sarp *et al.* [31]	224x224	6000	X-ray
Salama *et al.* [32]	220x220	2482	CT-scan
Bitto *et al.* [33]	224x224	7138	MRI
Prasetyo *et al.* [34]	224x224	5865	X-ray

2.2. Machine Learning Algorithms for Medical Image Classification

In recent years, various machine learning algorithms and methodologies have been widely applied in medical image classification and prediction for illness analysis and diagnosis, as shown in Table 2.

Table 2. Examples of machine learning algorithms application in medical image classification

Researcher	Details		
	Machine learning algorithms	*Target*	*Medical image type*
Prince *et al.* [35]	Decision tree, naïve Bayes, logistic regression, support vector machine, and k-nearest neighbors.	COVID-19 detection from chest X-ray images using CLAHE-YCrCb, LBP, and machine learning algorithms.	X-ray image
Singh *et al.* [36]	Support vector machine	Atherosclerotic plaque classification in carotid ultrasound images using machine learning.	Ultrasound
Zeng *et al.* [37]	Convolutional neural network.	Detection and processing of pulmonary nodules in CT images.	Computed Tomography
Jiang *et al.* [38]	Logistic regression, SVM, decision tree, k-NN, and stochastic gradient descent.	Magnetic resonance imaging brain tumor image classification based on five ML algorithms.	Computed Tomography

Table 2. (Cont…)

Researcher	Details		
	Machine learning algorithms	*Target*	*Medical image type*
Lehtonen *et al.* [39]	Linear regression, lasso, support vector machine, ridge, elastic net, logistic regression, random forest, and extreme gradient boosting.	Incremental prognostic value of downstream positron emission tomography (PET) perfusion imaging after coronary computed tomography angiography: a machine learning study.	Positron Emission Tomography
Nemoto *et al.* [40]	Random forest, naïve Bayes, support vector machine, k-nearest neighbors.	Evaluation of the performance of both machine learning models using PET and CT radionics for predicting recurrence following lung stereotactic body radiation therapy.	Hybrid modalities

2.3. Machine Learning and Its Applications in Medical Imaging

The development of machine learning techniques has greatly impacted policy-making, organizational transformation, and management processes in medicine, including diagnosis, nursing care, follow-up, and health management. This section highlights examples of machine learning applications to various medical image datasets widely used in medical imaging systems, as shown in Table 3.

Table 3. Application of machine learning algorithms in medical image analysis

Researcher	Details		
	Objective	*Dataset*	*Approaches to medical application*
Albataineh *et al.* [41]	Diagnosing the severity of COVID-19 from CT-scan images.	CT-scan image	Medical images
Islam *et al.* [42]	Using deep learning to identify COVID-19 and pneumonia from CT scan and X-ray images.	CT-scan image, X-ray image	
UmaMaheswaran *et al.* [43]	Early acute stroke detection using machine learning approach with Brain Computed Tomography.	Brain Computed Tomography scan (Brain CT)	
Anantharajan *et al.* [44]	MRI brain tumor detection using deep learning and machine learning approaches.	Magnetic Resonant Imaging (MRI)	
Morani *et al.* [45]	COVID-19 detection using CT images	CT-scan image	
Chaw *et al.* [46]	The accuracy of machine learning algorithms in predicting shock risk in dengue patients.	Physiological data of patients	Predictive analytics
Yang *et al.* [47]	Machine learning application in personalised lung cancer recurrence and survivability prediction.	The Cancer Genome Atlas (TCGA)	Personalized medicine
Barber *et al.*[48]	Natural language processing with machine learning to predict outcomes after ovarian cancer surgery.	CT-scan image	Natural language processing
Ala and Goli [49]	Assigning patients to the operating room based on fairness policy using machine learning.	Room data	Operational efficiency
Kavitha *et al.* [50]	Early-stage Alzheimer's disease prediction using machine learning models.	Magnetic Resonant Imaging (MRI)	Genomics and precision medicine
Kadum *et al.* [51]	Machine learning-based telemedicine framework to prioritize remote patients.	ECG, blood pressure	Remote monitoring and telemedicine

3. Results and Discussion

This section presents the results obtained from the research concept and framework shown in Fig. 1 and the datasets used in the study. Importantly, the research process and methodology were validated by Loei Rajabhat University's Research Ethics Committee (LRUREC No. H 009/2566).

3.1. Chest X-ray Image Processing and Model Development

3.1.1. Collect chest X-ray images

This study collected medical image datasets from four major public data repositories: Data.World, UCI Machine Learning Repository, Kaggle, and Reddit are popular datasets because they provide curated datasets for research and education. Since the chest X-ray (CXR) dataset has shown an important and empirical role in pneumonia screening and diagnosis, only CXR images were selected to ensure consistency and a comprehensive tool used clinically. The dataset includes images of pneumonia, lung infections, COVID-19, and healthy individuals, offering a comprehensive view of thoracic conditions. The images are provided in multiple formats, such as .jpg, .jpeg, and .png, to support various image processing and machine-learning applications.

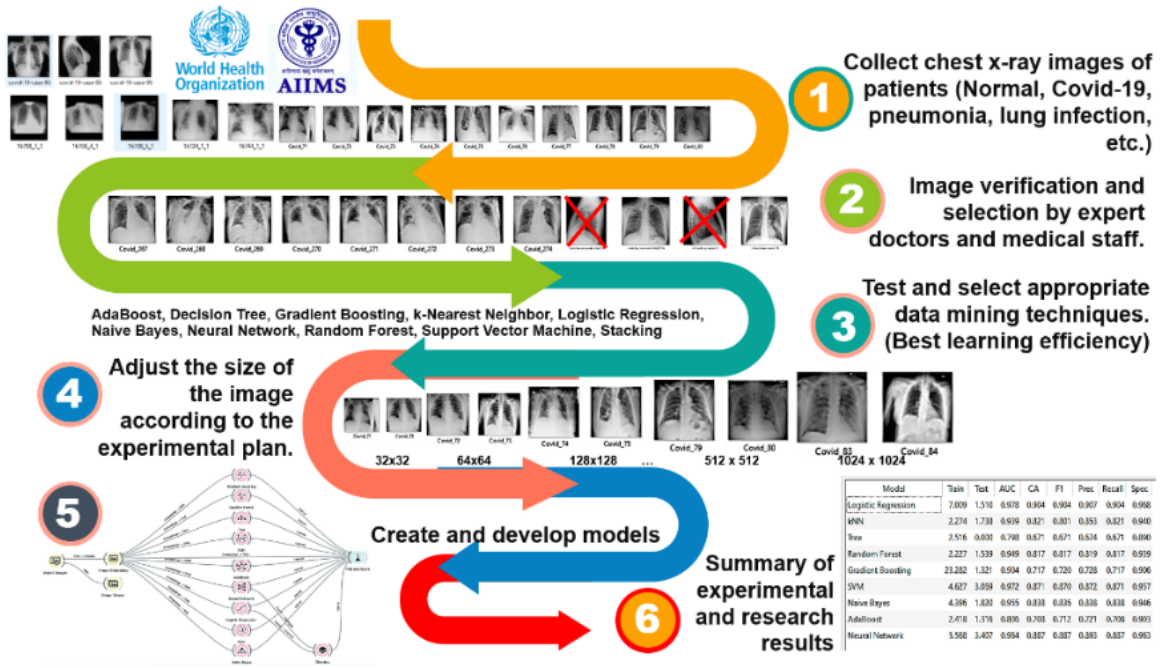

Fig. 1. Overview of the research process

3.1.2. Image verification and selection

Doctors and relevant officials will examine and verify all chest X-rays from the previous imaging data collection process for any abnormalities. After that, we will perform a computer screening of the images to select only those with medically acceptable completeness characteristics. The type of file used in this research will be in .jpg format only.

3.1.3. Adjust the size of the images

We plan to resize the images to 9 sizes together with the original images. The input image data for our machine learning process consists of images of sizes 1024x1024, 640x640, 512x512, 320x320, 299x299, 256x256, 128x128, 64x64, and 32x32. These images were resized according to the image sizes shown in Table 1. An image-resizing application was used to perform this operation. After resizing the images, the datasets of different sizes were stored in separate folders. Each dataset was divided into training and testing datasets.

3.2. Model simulation workflows in the Orange data mining software

In this section, we design a procedure to test the performance of machine learning algorithms on medical images of different sizes using the orange tools. Orange, a data mining software developed in 1997 by researchers at the University of Ljubljana, Slovenia [52], [53], was initially implemented in C++ and C to support machine learning algorithms. It was later redeveloped using the Python library, enhancing its functionality. Orange provides machine learning and data visualization capabilities through an intuitive, workflow-based interface.

According to the development team, this software is a graphical user interface focused on exploratory data analysis (EDA) instead of coding. Our experiment used 10 algorithms: gradient boosting, random forest, decision tree, support vector machine, AdaBoost, neural network, logistic regression, k-nearest neighbors, naive bays, and stacking, as shown in Fig. 2.

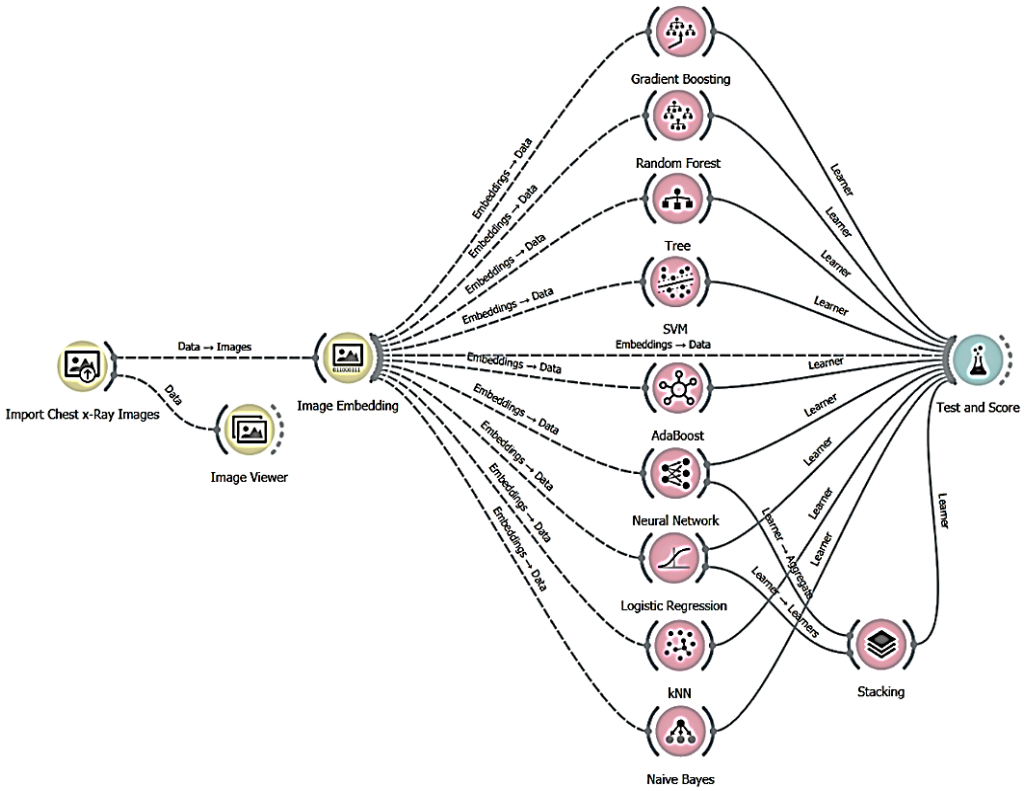

Fig. 2. Simulation workflows of performance testing of learning algorithms

3.3. Experiment results

The primary objective of this research was to identify the optimal dimensions for chest X-ray images to maximize the performance of machine learning models in accurately and efficiently detecting or predicting pneumonia cases. The study emphasized that selecting an appropriate image size plays a critical role in enhancing the capability of machine learning algorithms to process medical imaging data effectively. This optimization ensures precise identification of pneumonia cases and facilitates timely diagnosis, thereby supporting healthcare professionals in making informed clinical decisions. Such advancements are particularly significant in mitigating the spread and impact of the disease during the pandemic. The evaluation of the machine learning models utilized a comprehensive set of performance metrics, including training time, testing time, classification accuracy, F1-score, precision, recall, and specificity, as detailed in Table 4-Table 12. These metrics were employed to assess the robustness and reliability of the models, ensuring their suitability for real-world applications in medical image analysis. By adopting this systematic approach, the study contributes to developing efficient diagnostic tools, underscoring the potential of machine learning in addressing the challenges of pandemic management.

Table 4. 1024x1024 of Chest X-ray image sizes

Algorithms	Train time (s)	Test time (s)	Performance measurements				
			CA	*F1*	*Prec*	*Recall*	*Spec*
AdaBoost	602.56	5.35	0.69	0.69	0.69	0.69	0.84
DecisionTree	765.13	0.22	0.71	0.71	0.71	0.71	0.85
Gradient Boosting	34099.18	8.88	0.84	0.84	0.84	0.84	0.90
k-Nearest Neighbor	10.46	76.94	0.82	0.82	0.83	0.82	0.88
Logistic Regression	7565.94	5.11	0.87	0.87	0.87	0.87	0.93
Naive Bayes	26.67	6.93	0.65	0.66	0.69	0.65	0.86
Neural Network	922.32	13.48	0.88	0.88	0.88	0.88	0.93
Random Forest	80.28	5.53	0.79	0.78	0.79	0.79	0.87
SVM	529.42	155.13	0.59	0.61	0.67	0.59	0.85
Stacking	37853.22	5.60	0.77	0.75	0.80	0.77	0.82

Table 5. 640x640 of Chest X-ray image sizes

Algorithms	Train time (s)	Test time (s)	Performance measurements				
			CA	*F1*	*Prec*	*Recall*	*Spec*
AdaBoost	596.20	5.40	0.69	0.69	0.69	0.69	0.84
DecisionTree	858.82	0.11	0.71	0.71	0.71	0.71	0.85
Gradient Boosting	19891.14	8.66	0.84	0.84	0.84	0.84	0.90
k-Nearest Neighbor	10.67	81.91	0.82	0.82	0.82	0.82	0.88
Logistic Regression	7497.82	5.50	0.87	0.87	0.87	0.87	0.92
Naive Bayes	25.87	6.66	0.64	0.65	0.69	0.65	0.86
Neural Network	745.32	10.38	0.88	0.88	0.88	0.88	0.93
Random Forest	89.22	5.94	0.79	0.78	0.79	0.79	0.87
SVM	528.23	153.62	0.59	0.61	0.67	0.59	0.84
Stacking	49832.72	5.63	0.77	0.75	0.81	0.77	0.82

Table 6. 512x512 of Chest X-ray image sizes

Algorithms	Train time (s)	Test time (s)	Performance measurements				
			CA	*F1*	*Prec*	*Recall*	*Spec*
AdaBoost	757.08	6.83	0.69	0.69	0.69	0.69	0.84
DecisionTree	965.81	0.23	0.72	0.72	0.72	0.72	0.85
Gradient Boosting	24625.43	15.53	0.84	0.84	0.84	0.84	0.89
k-Nearest Neighbor	12.49	92.69	0.82	0.82	0.82	0.82	0.88
Logistic Regression	7433.73	5.42	0.87	0.87	0.87	0.87	0.93
Naive Bayes	37.18	10.18	0.65	0.65	0.69	0.65	0.86
Neural Network	807.58	10.35	0.88	0.88	0.88	0.88	0.92
Random Forest	103.68	6.75	0.78	0.78	0.78	0.79	0.87
SVM	585.65	181.15	0.58	0.61	0.68	0.58	0.85
Stacking	57606.97	24.25	0.77	0.73	0.79	0.76	0.81

Table 7. 320x320 of Chest X-ray image sizes

Algorithms	Train time (s)	Test time (s)	Performance measurements				
			CA	*F1*	*Prec*	*Recall*	*Spec*
AdaBoost	582.27	5.12	0.69	0.69	0.69	0.69	0.84
DecisionTree	765.47	0.09	0.71	0.71	0.71	0.71	0.85
Gradient Boosting	19867.69	8.62	0.84	0.84	0.84	0.84	0.9
k-Nearest Neighbor	9.92	79.24	0.82	0.82	0.82	0.82	0.88
Logistic Regression	7527.89	5.07	0.87	0.87	0.87	0.87	0.92
Naive Bayes	26.46	9.16	0.65	0.65	0.69	0.65	0.86
Neural Network	755.29	9.73	0.88	0.88	0.88	0.88	0.93
Random Forest	82.46	5.39	0.78	0.78	0.78	0.78	0.87
SVM	537.78	153.81	0.56	0.58	0.67	0.56	0.85
Stacking	3784	5.10	0.80	0.78	0.82	0.8	0.84

Table 8. 299x299 of Chest X-ray image sizes

Algorithms	Train time (s)	Test time (s)	Performance measurements				
			CA	*F1*	*Prec*	*Recall*	*Spec*
AdaBoost	595.71	5.20	0.69	0.69	0.69	0.69	0.84
DecisionTree	762.24	0.09	0.71	0.71	0.71	0.71	0.85
Gradient Boosting	19709.56	8.51	0.84	0.84	0.84	0.84	0.90
k-Nearest Neighbor	10.17	77.5	0.82	0.82	0.82	0.82	0.88
Logistic Regression	7484.95	5.05	0.87	0.87	0.87	0.87	0.93
Naive Bayes	26.67	7.94	0.65	0.66	0.69	0.65	0.86
Neural Network	748.23	9.68	0.87	0.87	0.87	0.87	0.92
Random Forest	81.78	5.84	0.79	0.78	0.79	0.79	0.87
SVM	525.85	149.08	0.63	0.64	0.70	0.63	0.86
Stacking	37317.35	5.60	0.79	0.77	0.81	0.79	0.83

Table 9. 256x256 of Chest X-ray image sizes

Algorithms	Train time (s)	Test time (s)	Performance measurements				
			CA	*F1*	*Prec*	*Recall*	*Spec*
AdaBoost	607.68	5.09	0.69	0.69	0.69	0.69	0.84
DecisionTree	762.81	0.09	0.71	0.71	0.71	0.71	0.85
Gradient Boosting	19612.05	8.53	0.84	0.84	0.84	0.84	0.90
k-Nearest Neighbor	10.16	79.66	0.82	0.82	0.82	0.82	0.88
Logistic Regression	7438.57	5.47	0.87	0.87	0.87	0.87	0.92
Naive Bayes	25.67	6.64	0.65	0.65	0.69	0.65	0.86
Neural Network	790.57	9.89	0.87	0.87	0.87	0.87	0.92
Random Forest	80.85	5.87	0.79	0.78	0.78	0.79	0.87
SVM	528.22	153.46	0.62	0.64	0.69	0.65	0.86
Stacking	37287.79	5.32	0.77	0.74	0.80	0.77	0.81

Table 10. 128x128 of Chest X-ray image sizes

Algorithms	Train time (s)	Test time (s)	Performance measurements				
			CA	*F1*	*Prec*	*Recall*	*Spec*
AdaBoost	561.59	5.16	0.68	0.68	0.68	0.68	0.68
DecisionTree	783.79	0.09	0.70	0.70	0.70	0.70	0.70
Gradient Boosting	19607.95	8.56	0.83	0.83	0.83	0.83	0.83
k-Nearest Neighbor	9.79	76.68	0.81	0.81	0.81	0.81	0.81
Logistic Regression	7357.06	5.18	0.86	0.86	0.86	0.86	0.86
Naive Bayes	25.93	6.76	0.63	0.64	0.68	0.63	0.63
Neural Network	834.19	10.39	0.88	0.88	0.88	0.88	0.88
Random Forest	78.83	5.31	0.77	0.77	0.77	0.77	0.77
SVM	532.35	153.05	0.58	0.60	0.67	0.58	0.58
Stacking	36207.23	7.62	0.80	0.79	0.83	0.80	0.80

Table 11. 64x64 of Chest X-ray image sizes

Algorithms	Train time (s)	Test time (s)	Performance measurements				
			CA	*F1*	*Prec*	*Recall*	*Spec*
AdaBoost	531.18	5.58	0.67	0.67	0.67	0.67	0.83
DecisionTree	815.64	0.10	0.69	0.69	0.69	0.69	0.84
Gradient Boosting	19863.64	9.51	0.82	0.82	0.82	0.82	0.88
k-Nearest Neighbor	9.75	78.30	0.80	0.80	0.80	0.80	0.87
Logistic Regression	7624.01	5.16	0.85	0.85	0.85	0.85	0.91
Naive Bayes	27.18	7.60	0.61	0.62	0.67	0.61	0.85
Neural Network	1008.36	10.48	0.86	0.86	0.86	0.86	0.92
Random Forest	77.19	5.80	0.77	0.76	0.77	0.77	0.86
SVM	540.69	156.23	0.52	0.55	0.64	0.52	0.83
Stacking	38075.32	5.14	0.76	0.74	0.79	0.76	0.80

Table 12. 32x32 of Chest X-ray image sizes

Algorithms	Train time (s)	Test time (s)	Performance measurements				
			CA	*F1*	*Prec*	*Recall*	*Spec*
AdaBoost	455.03	6.32	0.65	0.65	0.65	0.65	0.82
DecisionTree	851.42	0.22	0.67	0.67	0.67	0.67	0.83
Gradient Boosting	26197.50	8.80	0.79	0.79	0.79	0.79	0.87
k-Nearest Neighbor	9.81	77.15	0.77	0.77	0.77	0.77	0.85
Logistic Regression	7884.34	5.19	0.82	0.82	0.82	0.82	0.90
Naive Bayes	26.77	6.91	0.61	0.61	0.63	0.61	0.83
Neural Network	1059.16	11.20	0.83	0.83	0.83	0.83	0.91
Random Forest	72.99	5.51	0.75	0.74	0.75	0.75	0.85
SVM	528.20	154.98	0.42	0.43	0.52	0.42	0.79
Stacking	50798.59	5.29	0.74	0.71	0.78	0.74	0.78

3.4. Discussion

To determine the most suitable chest X-ray image size for use in the machine learning process for developing a pneumonia infection prediction model. There are mainly two goals to consider: the learning efficiency of each algorithm and the time required to train and test to evaluate the model. Gradient boosting, random forest, decision tree, support vector machine, AdaBoost, neural network, logistic regression, k-nearest neighbors, naive bays, and stacking are some of the most common machine learning methods used in developing models. The learning efficiency metrics were compared to the classification accuracy (CA), F-1, precision (Prec), and recall. The time efficiency of the prediction model was measured by the time it took to train and test the various models.

3.4.1. Impact of Image size on Neural Network Performance for Chest X-ray image Prediction

The progress of machine learning methods has greatly enhanced the precision and effectiveness of predictive models in analyzing medical images. In this research, we assessed the efficacy of multiple algorithms; however, the artificial neural network algorithm has displayed the most tremendous significance for classifying chest X-ray images, as indicated in Tables 4–12. The algorithm attained an average accuracy of 87.00%, showcasing its reliability in distinguishing between various medical conditions. This achievement is due to the model's capacity to learn intricate patterns in chest X-ray data accurately. Nevertheless, its effectiveness is affected by various factors, including the complexity of the neural network, design decisions (e.g., convolutional layers for handling images), and optimization methods like backpropagation, dropout, and regularization. These factors are essential for improving the model's ability to extract features and its overall predictive effectiveness.

A primary goal of this research was to assess how image size affects the learning efficiency of neural networks. The experimental findings show a notable decrease in model performance when the image resolution is greatly lowered. In particular, when the input dimension was reduced to 32×32 pixels, the model's accuracy fell to 83%, as indicated in Table 12. This decline in precision is probably caused by the loss of essential visual elements, which hinders the model's ability to distinguish between medical conditions accurately. Since neural networks depend on intricate image representations for accurate classification, reduced resolutions restrict the model's ability to identify critical diagnostic characteristics. On the other hand, enhancing the image resolution retains additional essential details, allowing the model to examine and learn more efficiently. For instance, when the image size was enlarged, the algorithm's accuracy improved to 88%, as indicated in Tables 4–12, demonstrating that higher resolutions contribute to better feature extraction and classification accuracy. Despite the overall positive correlation between image size and model performance, the findings reveal a point of diminishing returns. While increasing resolution improves prediction accuracy to a point, extending it further past a limit results in only slight enhancements. In particular, enlarging the image dimensions from 128×128 to 1024×1024 pixels led to minimal improvements in accuracy. This implies that after the resolution reaches a level adequate for extracting important features, further enhancements offer minimal extra advantage. Beyond a certain threshold, increasing resolution does not significantly improve classification accuracy, emphasizing the importance of selecting an appropriate image size for efficient and effective medical image analysis.

3.4.2. Impact of Image Size on Training and Testing Time in Predictive Model for Pneumonia Chest X-ray Classification

The system requires precision, accuracy, and optimal computational efficiency in the training and testing phases to develop predictive models for pneumonia diagnosis effectively. A research analysis investigates how changes in image dimensions affect the computational demands of model training and testing activities while determining how such changes affect model implementation performance. The experimental findings demonstrate that higher resolution settings in chest X-ray images result in longer durations throughout the training and testing model procedures. Complex neural network architectures are necessary for processing extensive image details in larger images. The training duration and computational processing time grow proportionally with image size expansion. The neural network model that processed 299×299pixel images displayed the quickest efficiency during testing and training, lasting 748.23 seconds. The processing speed shows that improved image features can be extracted from higher resolutions yet requires a precise balance between performance accuracy and system operation speed.

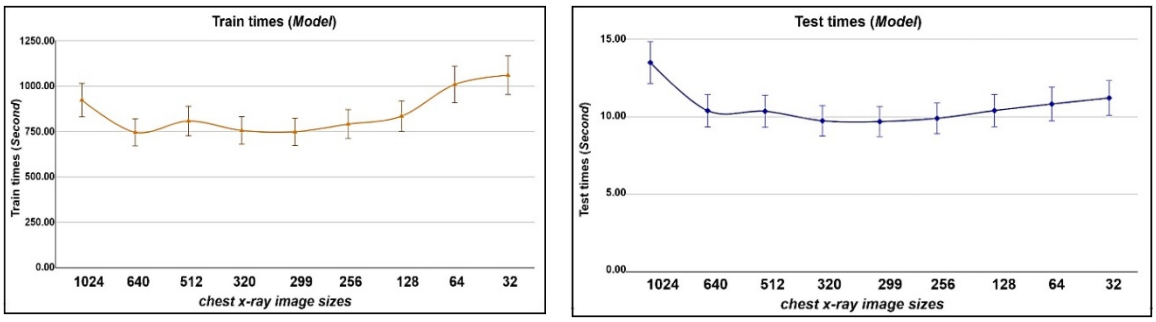

(a) Train times (Model) (b) Test time (Model)

Fig. 3. Comparison of training and testing time trends

Decreasing picture resolution results in more straightforward features that may speed up calculations. Lowering the image resolution reduces diagnostic accuracy because vital diagnostic factors become harder to detect, which causes a decrease in prediction performance. Our research demonstrates that small-sized chest X-ray images maintain prolonged training and testing durations while preventing the model from detecting essential patterns since detail is too sparse, as illustrated in Fig. 3. The reduction in image size provides a computational benefit. Still, it leads to losing vital medical characteristics needed for precise classification. The research findings demonstrate that oversized or undersized images lead to longer periods required for the training and testing process. Importantly, the results demonstrate why selecting an appropriate image resolution matters because it balances the model's performance with efficient computational processing. While higher resolutions enhance learning capabilities, they also demand longer training and testing times. Meanwhile, excessively small images hinder model performance by removing critical diagnostic details. Therefore, an optimal image size must be selected to balance predictive accuracy and computational efficiency, ensuring effective and resource-conscious model development for pneumonia chest X-ray classification.

Our near future work will focus on tailoring our chest X-ray machine learning models to regional healthcare contexts, including understanding local needs, tailoring image processing techniques to the quality of commonly available X-rays, and developing a user-friendly interface with localization and language support. It is important to optimize the application for resource-constrained environments, taking into account efficient computing and offline functionality. We are very aware that rapid and comprehensive pilot testing in targeted areas will improve the validation of the application, and feedback from local healthcare providers will guide further improvements. Comprehensive training of healthcare professionals will ensure the system is properly functional. Continuous validation and iterative improvement are needed to adapt the application to changing healthcare needs, ultimately improving the diagnostics of COVID-19 and other respiratory conditions.

4. Conclusion

This study aimed to determine the most suitable chest X-ray image size for machine-learning models in pneumonia infection prediction by evaluating both learning efficiency and computational time. Artificial neural networks demonstrated the highest classification accuracy among machine learning methods, averaging 87.00%. The results indicated that image resolution significantly impacts model performance, with lower resolutions (e.g., 32×32 pixels) reducing accuracy due to loss of essential diagnostic features. Higher resolutions (e.g., 299×299 pixels) improved predictive capability. However, increasing resolution beyond a certain point yielded minimal accuracy gains, highlighting the need for an optimal balance between resolution and computational efficiency. Furthermore, the study revealed that higher-resolution images enhance feature extraction and increase training and testing time. The computational demands of processing larger images must be weighed against the benefits of improved model accuracy. An optimal image size ensures efficient training and reliable classification, balancing precision and system performance. Future work will focus on adapting the machine learning model to regional healthcare contexts by optimizing image processing techniques, integrating localization and language support, and ensuring resource-efficient computing. Pilot testing in target areas and continuous feedback from healthcare professionals will enhance validation and refinement. Ultimately, this research contributes to developing a practical and scalable pneumonia detection model, improving diagnostic capabilities for COVID-19 and other respiratory conditions.

Acknowledgment

Financial support for this research has been provided under the grant RESEARCH FUNDING from the Research Fund, Loei Rajabhat University. The authors would like to thank Tawsifur Rahman, Muhammad Chowdhury, and Amith Khandakar for the chest X-ray image dataset from www.kaggle.com/datasets/-tawsifurrahman/covid19-radiography-database.

Declarations

Author contribution. Conceptualization, Kriengsak Yothapakdee; Data curation, Kriengsak Yothapakdee and Tanunchai Boonnuk; Funding ac-quisition, Kriengsak Yothapakdee; Investigation, Kriengsak Yothapakdee, Yosawaj Pugtao, Sarawoot Charoenkhun and Kreangsak Tamee; Methodology, Kriengsak Yothapakdee, Tanunchai Boonnuk and Kreangsak Tamee; Writing-original draft, Kriengsak Yothapakdee; Writing-review & editing, Kriengsak Yothapakdee and Tanunchai Boonnuk.
Funding statement. This research received no external funding.
Conflict of interest. The authors declare no conflict of interest.
Additional information. No additional information is available for this paper.

References

[1] M. Bundea and G. M. Danciu, "Pneumonia Image Classification Using DenseNet Architecture," *Information*, vol. 15, no. 10, p. 611, Oct. 2024, doi: 10.3390/info15100611.

[2] S. W. Teklu and B. S. Kotola, "Insight into the treatment strategy on pneumonia transmission with asymptotic carrier stage using fractional order modeling approach," *Comput. Methods Programs Biomed. Updat.*, vol. 5, p. 100134, Jan. 2024, doi: 10.1016/j.cmpbup.2024.100134.

[3] "Pneumonia," *Wold Health Organization*, 2025. [Online]. Available at: https://www.who.int/health-topics/pneumonia/#tab=tab_1.

[4] S. Santos *et al.*, "The SARS-CoV-2 test scale-up in the USA: an analysis of the number of tests produced and used over time and their modelled impact on the COVID-19 pandemic," *Lancet Public Heal.*, vol. 10, no. 1, pp. e47–e57, Jan. 2025, doi: 10.1016/S2468-2667(24)00279-2.

[5] J. Zhang, X. Dong, G. Liu, and Y. Gao, "Risk and Protective Factors for COVID-19 Morbidity, Severity, and Mortality," *Clin. Rev. Allergy Immunol.*, vol. 64, no. 1, pp. 90–107, Jan. 2022, doi: 10.1007/s12016-022-08921-5.

[6] "Infection prevention and control guideline for coronavirus disease 2019 (COVID-19): Executive summary, 21 December 2023," *World Health Organization (WHO)*, 2023. [Online]. Available at: https://www.who.int/publications/i/item/WHO-2019-nCoV-IPC-guideline-summary-2023.4.

[7] K. Cheng, C. Wu, S. Gu, Y. Lu, H. Wu, and C. Li, "WHO declares end of COVID-19 global health emergency: lessons and recommendations from the perspective of ChatGPT/GPT-4," *Int. J. Surg.*, vol. 109, no. 9, pp. 2859–2862, May 2023, doi: 10.1097/JS9.0000000000000521.

[8] A. S. M. Roknuzzaman, R. Sarker, and M. R. Islam, "The World Health Organization has endorsed COVID-19 is no longer a global public health emergency: How they took this step and what we should do right now?," *Int. J. Health Plann. Manage.*, vol. 38, no. 5, pp. 1595–1598, Sep. 2023, doi: 10.1002/hpm.3668.

[9] C. Tian, L. Balmer, and X. Tan, "COVID-19 lessons to protect populations against future pandemics by implementing PPPM principles in healthcare," *EPMA J.*, vol. 14, no. 3, pp. 329–340, Jul. 2023, doi: 10.1007/s13167-023-00331-7.

[10] M. M. Ibrahim, "Chest X-ray Findings in Community-acquired Pneumonia," *Mustansiriya Med. J.*, vol. 22, no. 2, pp. 217–223, Jul. 2023, doi: 10.4103/mj.mj_52_23.

[11] J. Yao *et al.*, "EVA-X: A Foundation Model for General Chest X-ray Analysis with Self-supervised Learning," *arxiv Artif. Intell.*, pp. 1–27, 2024, [Online]. Available at: http://arxiv.org/abs/2405.05237.

[12] Muhammad Suliman, F. Malik, M. Q. Khan, Ashraf Ullah, N. Rahman, and S. K. Shah, "A Convolutional Neural Network (CNN) Based Framework for Enhanced Diagnosis and Classification of COVID-19 Pneumonia," *VAWKUM Trans. Comput. Sci.*, vol. 12, no. 2, pp. 220–240, Dec. 2024, doi: 10.21015/vtcs.v12i2.1999.

[13] M. I. U. Haque, A. K. Dubey, I. Danciu, A. C. Justice, O. S. Ovchinnikova, and J. D. Hinkle, "Effect of image resolution on automated classification of chest X-rays," *J. Med. Imaging*, vol. 10, no. 04, p. 044503, Aug. 2023, doi: 10.1117/1.JMI.10.4.044503.

[14] S. Rajaraman, F. Yang, G. Zamzmi, Z. Xue, and S. Antani, "Assessing the Impact of Image Resolution on Deep Learning for TB Lesion Segmentation on Frontal Chest X-rays," *Diagnostics*, vol. 13, no. 4, p. 747, Feb. 2023, doi: 10.3390/diagnostics13040747.

[15] A. Olar, A. Biricz, Z. Bedőházi, B. Sulyok, P. Pollner, and I. Csabai, "Automated prediction of COVID-19 severity upon admission by chest X-ray images and clinical metadata aiming at accuracy and explainability," *Sci. Rep.*, vol. 13, no. 1, p. 4226, Mar. 2023, doi: 10.1038/s41598-023-30505-2.

[16] M. Pal, S. Parija, G. Panda, S. Mishra, R. K. Mohapatra, and K. Dhama, "COVID-19 Prognosis from Chest X-ray Images by using Deep Learning Approaches: A Next Generation Diagnostic Tool," *J. Pure Appl. Microbiol.*, vol. 17, no. 2, pp. 919–930, Jun. 2023, doi: 10.22207/JPAM.17.2.20.

[17] S. M. Baik, K. S. Hong, and D. J. Park, "Deep learning approach for early prediction of COVID-19 mortality using chest X-ray and electronic health records," *BMC Bioinformatics*, vol. 24, no. 1, p. 190, May 2023, doi: 10.1186/s12859-023-05321-0.

[18] C. C. Ukwuoma *et al.*, "Deep learning framework for rapid and accurate respiratory COVID-19 prediction using chest X-ray images," *J. King Saud Univ. - Comput. Inf. Sci.*, vol. 35, no. 7, p. 101596, Jul. 2023, doi: 10.1016/j.jksuci.2023.101596.

[19] B. B. Reddy, M. V. Sudhakar, P. R. Reddy, and P. R. Reddy, "Ensemble deep honey architecture for COVID-19 prediction using CT scan and chest X-ray images," *Multimed. Syst.*, vol. 29, no. 4, pp. 2009–2035, Aug. 2023, doi: 10.1007/s00530-023-01072-3.

[20] Z. Liu and L. Shen, "CECT: Controllable ensemble CNN and transformer for COVID-19 image classification," *Comput. Biol. Med.*, vol. 173, p. 108388, May 2024, doi: 10.1016/j.compbiomed.2024.108388.

[21] T. Chen *et al.*, "A vision transformer machine learning model for COVID-19 diagnosis using chest X-ray images," *Healthc. Anal.*, vol. 5, p. 100332, Jun. 2024, doi: 10.1016/j.health.2024.100332.

[22] A. Echtioui and Y. Ben Ayed, "Automated detection of COVID-19 based on transfer learning," *Multimed. Tools Appl.*, vol. 83, no. 11, pp. 33731–33751, Sep. 2023, doi: 10.1007/s11042-023-17023-z.

[23] M. Abdullah, F. berhe Abrha, B. Kedir, and T. Tamirat Tagesse, "A Hybrid Deep Learning CNN model for COVID-19 detection from chest X-rays," *Heliyon*, vol. 10, no. 5, p. e26938, Mar. 2024, doi: 10.1016/j.heliyon.2024.e26938.

[24] K. Akyol, "ETSVF-COVID19: efficient two-stage voting framework for COVID-19 detection," *Neural Comput. Appl.*, vol. 36, no. 29, pp. 18277–18295, Oct. 2024, doi: 10.1007/s00521-024-10150-0.

[25] D. I. Morís, J. de Moura, J. Novo, and M. Ortega, "Adapted generative latent diffusion models for accurate pathological analysis in chest X-ray images," *Med. Biol. Eng. Comput.*, vol. 62, no. 7, pp. 2189–2212, Jul. 2024, doi: 10.1007/s11517-024-03056-5.

[26] S. Asif, Y. Wenhui, K. Amjad, H. Jin, Y. Tao, and S. Jinhai, "Detection of COVID-19 from chest X-ray images: Boosting the performance with convolutional neural network and transfer learning," *Expert Syst.*, vol. 40, no. 1, p. e13099, Jan. 2023, doi: 10.1111/exsy.13099.

[27] S. Shastri, I. Kansal, S. Kumar, K. Singh, R. Popli, and V. Mansotra, "CheXImageNet: a novel architecture for accurate classification of Covid-19 with chest x-ray digital images using deep convolutional neural networks," *Health Technol. (Berl).*, vol. 12, no. 1, pp. 193–204, Jan. 2022, doi: 10.1007/s12553-021-00630-x.

[28] A. Hayat, P. Baglat, F. Mendonça, S. S. Mostafa, and F. Morgado-Dias, "Novel Comparative Study for the Detection of COVID-19 Using CT Scan and Chest X-ray Images," *Int. J. Environ. Res. Public Health*, vol. 20, no. 2, p. 1268, Jan. 2023, doi: 10.3390/ijerph20021268.

[29] M. M. M. Alghamdi, M. Y. H. Dahab, and N. H. A. Alazwary, "Enhancing deep learning techniques for the diagnosis of the novel coronavirus (COVID-19) using X-ray images," *Cogent Eng.*, vol. 10, no. 1, Dec. 2023, doi: 10.1080/23311916.2023.2181917.

[30] I. Kanjanasurat, K. Tenghongsakul, B. Purahong, and A. Lasakul, "CNN–RNN Network Integration for the Diagnosis of COVID-19 Using Chest X-ray and CT Images," *Sensors*, vol. 23, no. 3, p. 1356, Jan. 2023, doi: 10.3390/s23031356.

[31] S. Sarp *et al.*, "An XAI approach for COVID-19 detection using transfer learning with X-ray images," *Heliyon*, vol. 9, no. 4, p. e15137, Apr. 2023, doi: 10.1016/j.heliyon.2023.e15137.

[32] G. M. Salama, A. Mohamed, and M. K. Abd-Ellah, "COVID-19 classification based on a deep learning and machine learning fusion technique using chest CT images," *Neural Comput. Appl.*, vol. 36, no. 10, pp. 5347–5365, Apr. 2024, doi: 10.1007/s00521-023-09346-7.

[33] A. K. Bitto, M. H. I. Bijoy, S. Yesmin, I. Mahmud, M. J. Mia, and K. B. B. Biplob, "Tumor-Net: convolutional neural network modeling for classifying brain tumors from MRI images," *Int. J. Adv. Intell. Informatics*, vol. 9, no. 2, p. 148, Apr. 2023, doi: 10.26555/ijain.v9i2.872.

[34] S. Y. Prasetyo, G. Z. Nabiilah, Z. N. Izdihar, and S. M. Isa, "Pneumonia Detection on X-Ray Imaging using Softmax Output in Multilevel Meta Ensemble Algorithm of Deep Convolutional Neural Network Transfer Learning Models," *Int. J. Adv. Intell. Informatics*, vol. 9, no. 2, p. 319, Jul. 2023, doi: 10.26555/ijain.v9i2.884.

[35] R. Prince, Z. Niu, Z. Y. Khan, M. Emmanuel, and N. Patrick, "COVID-19 detection from chest X-ray images using CLAHE-YCrCb, LBP, and machine learning algorithms," *BMC Bioinformatics*, vol. 25, no. 1, p. 28, Jan. 2024, doi: 10.1186/s12859-023-05427-5.

[36] S. Singh, P. K. Jain, N. Sharma, M. Pohit, and S. Roy, "Atherosclerotic plaque classification in carotid ultrasound images using machine learning and explainable deep learning," *Intell. Med.*, vol. 4, no. 2, pp. 83–95, May 2024, doi: 10.1016/j.imed.2023.05.003.

[37] Q. Zeng, W. Sun, J. Xu, W. Wan, and L. Pan, "Machine Learning-Based Medical Imaging Detection and Diagnostic Assistance," *Int. J. Comput. Sci. Inf. Technol.*, vol. 2, no. 1, pp. 36–44, Mar. 2024, doi: 10.62051/ijcsit.v2n1.05.

[38] Song Jiang, Yuan Gu, and Ela Kumar, "Magnetic Resonance Imaging (MRI) Brain Tumor Image Classification Based on Five Machine Learning Algorithms," *Cloud Comput. Data Sci.*, pp. 122–133, May 2023, doi: 10.37256/ccds.4220232740.

[39] E. Lehtonen *et al.*, "Incremental prognostic value of downstream positron emission tomography perfusion imaging after coronary computed tomography angiography: a study using machine learning," *Eur. Hear. J. - Cardiovasc. Imaging*, vol. 25, no. 2, pp. 285–292, Jan. 2024, doi: 10.1093/ehjci/jead246.

[40] H. Nemoto *et al.*, "Evaluation of the performance of both machine learning models using PET and CT radiomics for predicting recurrence following lung stereotactic body radiation therapy: A single-institutional study," *J. Appl. Clin. Med. Phys.*, vol. 25, no. 7, p. e14322, Jul. 2024, doi: 10.1002/acm2.14322.

[41] Z. Albataineh, F. Aldrweesh, and M. A. Alzubaidi, "COVID-19 CT-images diagnosis and severity assessment using machine learning algorithm," *Cluster Comput.*, vol. 27, no. 1, pp. 547–562, Feb. 2024, doi: 10.1007/s10586-023-03972-5.

[42] N. Islam *et al.*, "COVID-19 and Pneumonia detection and web deployment from CT scan and X-ray images using deep learning," *PLoS One*, vol. 19, no. 7, p. e0302413, Jul. 2024, doi: 10.1371/journal.pone.0302413.

[43] S. K. UmaMaheswaran, F. Ahmad, R. Hegde, A. M. Alwakeel, and S. Rameem Zahra, "Enhanced non-contrast computed tomography images for early acute stroke detection using machine learning approach," *Expert Syst. Appl.*, vol. 240, p. 122559, Apr. 2024, doi: 10.1016/j.eswa.2023.122559.

[44] S. Anantharajan, S. Gunasekaran, T. Subramanian, and V. R, "MRI brain tumor detection using deep learning and machine learning approaches," *Meas. Sensors*, vol. 31, p. 101026, Feb. 2024, doi: 10.1016/j.measen.2024.101026.

[45] K. Morani, E. K. Ayana, and D. Unay, "Covid-19 detection using modified xception transfer learning approach from computed tomography images," *Int. J. Adv. Intell. Informatics*, vol. 9, no. 3, p. 524, Nov. 2023, doi: 10.26555/ijain.v9i3.1432.

[46] J. K. Chaw *et al.*, "A predictive analytics model using machine learning algorithms to estimate the risk of shock development among dengue patients," *Healthc. Anal.*, vol. 5, p. 100290, Jun. 2024, doi: 10.1016/j.health.2023.100290.

[47] Y. Yang, L. Xu, L. Sun, P. Zhang, and S. S. Farid, "Machine learning application in personalised lung cancer recurrence and survivability prediction," *Comput. Struct. Biotechnol. J.*, vol. 20, pp. 1811–1820, Jan. 2022, doi: 10.1016/j.csbj.2022.03.035.

[48] E. L. Barber, R. Garg, C. Persenaire, and M. Simon, "Natural language processing with machine learning to predict outcomes after ovarian cancer surgery," *Gynecol. Oncol.*, vol. 160, no. 1, pp. 182–186, Jan. 2021, doi: 10.1016/j.ygyno.2020.10.004.

[49] A. Ala and A. Goli, "Incorporating machine learning and optimization techniques for assigning patients to operating rooms by considering fairness policies," *Eng. Appl. Artif. Intell.*, vol. 136, p. 108980, Oct. 2024, doi: 10.1016/j.engappai.2024.108980.

[50] C. Kavitha, V. Mani, S. R. Srividhya, O. I. Khalaf, and C. A. Tavera Romero, "Early-Stage Alzheimer's Disease Prediction Using Machine Learning Models," *Front. Public Heal.*, vol. 10, p. 853294, Mar. 2022, doi: 10.3389/fpubh.2022.853294.

[51] S. Y. Kadum *et al.*, "Machine learning-based telemedicine framework to prioritize remote patients with multi-chronic diseases for emergency healthcare services," *Netw. Model. Anal. Heal. Informatics Bioinforma.*, vol. 12, no. 1, p. 11, Jan. 2023, doi: 10.1007/s13721-022-00407-w.

[52] F. Tscherne, N. Wilke, B. Schachenhofer, K. Roux, and G. Tavlaridis, "The thermo lignum ecological insect pest eradication process: The effects on gilded and painted wooden objects," *Int. J. Conserv. Sci.*, vol. 7, no. SpecialIssue1, pp. 295–300, 2016, [Online]. Available at: https://www.jmlr.org/papers/volume14/demsar13a/demsar13a.pdf.

[53] T. Hočevar and B. Zupan, "Conformal Prediction and its Integration within Visual Analytics Toolbox," *Proc. Mach. Learn. Res.*, vol. 152, no. 2008, pp. 286–293, 2021, [Online]. Available at: https://proceedings.mlr.press/v152/hocevar21a/hocevar21a.pdf.